ESTA JOURNAL
Energy Storage Technology and Applications

Article

jurnal.uns.ac.id/esta

Characterization of $FeMnPO_4$ as Precursor to $LiFeMnPO_4$: Effect of Reaction pH

H. N. Wibowo[1], M. Arinawati[2], Khairuddin[1], C.S. Yudha[2,3,*]

1. Department of Physics, Faculty of Mathematics and Science Universitas Sebelas Maret
2. Chemical Engineering Department, Vocational School, Universitas Sebelas Maret, Jl. Kol. Sutarto 150K Jebres, Surakarta 57126, Indonesia
3. Centre of Excellence for Electrical Energy Storage Technology, Universitas Sebelas Maret, Jl. Slamet Riyadi 435, Surakarta 57146, Indonesia

* Corresponding author: corneliussyudha@staff.uns.ac.id

doi : https://dx.doi.org/10.20961/esta.v2i2.67675

Received: 11-24-2022; Revised: 01-04-2023; Accepted: 03-01-2023; Published: 03-01-2023

ABSTRACT: The development of the battery market demands batteries with high-performance ability. One of the promising materials to be developed as novel commercial LIBs is Lithium Ferro Manganese Phosphate. Lithium Ferro Manganese Phosphate ($LiFe_{0.5}Mn_{0.5}PO_4$)/LFMP battery can be achieved by preparing the precursors using the co-precipitation method. In this study, the Variation of pH of 2,3, and 4 was used to obtain LFMP precursor $Fe_{0.5}Mn_{0.5}PO_4$while the result was analyzed using characterization techniques. In the FTIR test, there are groups of bending and stretching bonds from H_2O, P-O bonds originating from phosphate groups, and Fe-O bonds stretching. In the SEM-EDX test, samples at pH 2 and 3 experienced agglomerations which reduced battery capacity. The percentage of Fe, Mn, P, and O atoms in samples at pH 2 and 3 did not meet stoichiometric calculations due to the side reactions which affected the ratio of Mn and P atoms. In the XRD test, the FeMnPO4 precursor was still in an amorphous phase so it was still difficult to determine the exact crystallization peak. According to the literature. This is partly caused by the temperature and the longtime of stirring. In the TG-DTA test, the pH 2 sample had an initial mass difference of 0.76 grams and underwent an endothermic reaction at a temperature range of 26°- 131°C then took place exothermic in the range of 132-241°C. In the pH 3 sample, an initial mass difference of 1.71 gram and, the exothermic peak was recorded at temperatures of 70.9°C, and 651.88°C. Meanwhile, the endothermic peak was recorded at 701.95°C. The pH 4 sample has a final-initial mass difference of 5.27 grams and the sample undergoes an exothermic reaction in the range of 40-91.73°C and 274.27-297.75°C.

Keywords: Li-ion battery, cobalt-free cathode, crystallization, Characterization, Precipitation.

1. Introduction

Renewable energy sources have become a hot topic of discussion in recent years. This renewable energy source is expected to provide benefits and advantages for users and the environment in the future. One of the renewable energies that is often used is the battery. Batteries

are generally used as a source as well as storage of electrical energy in various devices such as electronic devices, motorized vehicles, and other devices that require secondary energy storage[1].

Lithium-Ion batteries are the talk of the town when discussing secondary energy sources. A secondary battery is a type of battery that utilizes a reversible chemical reaction. Currently, lithium-ion batteries are batteries that are needed for electrical energy needs in cell phones, mp3 players, and others. In addition, lithium-ion batteries are needed, especially for vehicles that have an energy source from electric energy / electric vehicles. The demand for lithium-ion batteries is always increasing from year to year[2]. This is due to the ability to store energy longer and also the increased battery life cycle. Lithium-ion battery is a battery that can store electrical energy for a long time. One of the factors that affect the properties of lithium-ion batteries is the quality of the electrode material (anode/cathode)[3]. One effort to improve the performance of the battery is to improve the quality of the electrodes used.

The lithium-ion battery has four important parts in it, namely the positive electrode which is called the cathode, the negative electrode which is called the anode, the electrolyte and the separator [4]. The material that is often used as an anode is graphite material. While the materials that are often used as cathodes are generally made of lithium cobalt oxide (LCO), lithium manganese oxide (LMO), lithium Ferro phosphate (LFP), and many more[5].

Lithium-ion battery research has progressed over the years. Things that are often discussed and varied in lithium battery research include the type of electrodes used, how to make precursors and active materials, characterization, and charge tests to determine electrochemical properties[6].

With so many variables being tested, important information about the lithium-ion battery obtained also varies. Each lithium-ion battery has certain properties based on the cathode active material used and how it is made [7]. In this research, we will discuss the manufacture and characterization of Lithium Ferro Manganese Phosphate ($LiFe_{0.5}Mn_{0.5}PO_4$) battery precursors using the co-precipitation method.

2. Experimental Method

2.1 Material

The materials used are ferrous sulfate heptahydrate ($FeSO_4.7H_2O$) (Nikosia, Indonesia), manganese sulfate monohydrate ($MnSO_4.H_2O$) (Merck, Germany), Sodium hydroxide (NaOH) (Asahimas, Indonesia), phosphoric acid (H_3PO_4) (Merck, Germany), and Lithium Carbonate (Li_2CO_3, Sichuan Brivo Chemical Co. Ltd, China).

2.2 Methodology

2.2.1 Synthesis of $FeMnPO_4$

The $FeMnPO_4$ precursor was prepared using the co-precipitation method with a Fe: Mn: PO_4 ratio of 0.5: 0.5: 1. Solutions of 1 M $FeSO_4$ and 1 M $MnSO_4$ were prepared by dissolving $FeSO_4.7H_2O$ and $MnSO_4.H_2O$ respectively in 50 ml of water and then stirring using a magnetic stirrer. The $FeSO_4$ solution was filtered to separate the precipitate using filter paper. Then the filtered $FeSO_4$ solution was mixed with $MnSO_4$ and H_3PO_4 solutions and stirred for 4 hours at 120 C. 1 M NaOH solution was prepared by dissolving solid NaOH in 50 ml of water.

During the stirring process, the NaOH solution is added little by little to the mixture while observing the pH of the mixture. In this study, variations in the pH of the mixed solution were 2, 3, and 4 respectively. The process of stirring and

adding the NaOH solution was stopped when the pH of the mixture changed to 2, 3, and 4. Then the mixed solution was filtered and washed until the pH was changed to 7. After that, the precipitate formed was dried in an oven for 24 hours to reduce the water content contained in the slurry so that the final result obtained was $FeMnPO_4$ precursor powder.

2.2.2 Characterization of materials and electrochemical performance test.

Powder X-ray diffraction (XRD) was used to evaluate the crystal structure of the obtained powder materials. These three samples were tested using a mini diffractometer (MTI, USA) with CuKα radiation = 1.5418 in the range of 17-67°. SEM (Scanning Electron Microscope) testing was also carried out at 5000x magnification (JEOL, Japan). The Fourier transfer infrared (FTIR) test was also applied to samples operating with a wavelength range of 400-4000 cm^{-1} at room temperature (Shimadzu, Japan). To study the thermal decomposition of powder material, a gravimetric/thermal differential thermal analysis (TG/DTA, Shimadzu DTG-60 Japan) was performed.

3. Results and Discussion

3.1 Characterization of the Precursors

Figure 1. is an image of the SEM test results of $FeMnPO_4$ precursors made with co-precipitation pH 2. Precursor characteristic tests were carried out at 500x, 1000x, and 5000x magnification, respectively. In Figure 1. the precursor with pH 2 shows that there is still a lot of agglomeration occurring compared to the precursor powder with pH 3 and 4. Table 4.1 is the result of EDX characterization testing on the $FeMnPO_4$ precursor variant pH 2. In the table, it is known that the element with the largest weight is element O with mass percentage = 52.68 ± 4.05%, then Fe = 28.07 ± 5.36%, followed by element P = 19.05 ± 2.15%, and lastly Mn = 0.20 ± 0.60 % Meanwhile, the percentage of Mn atoms in the samples with variations in pH 2 was not by stoichiometric calculations[8].

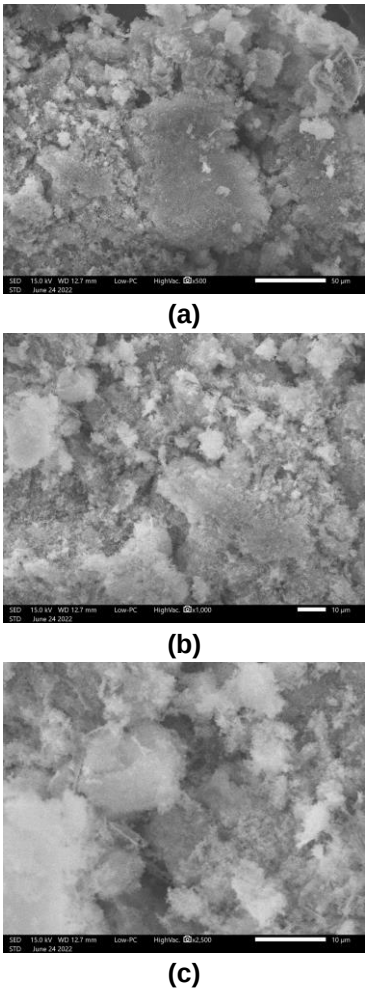

Figure 1. SEM pattern of the precursor of $FeMnPO_4$ (pH =2) with magnifications (a) 500x, (b) 1000x, and (c) 5000x

Table 1. EDX analysis of $FeMnPO_4$ (Ph = 2)

Elements	%Mass	%Atom
O	52.68±4,05	74,60±5,74
P	19,05±2,15	13,93±1,57
Mn	0,20±0,60	0,08±0,25
Fe	28,07±5,36	11,39±2,18

Figure 2. the result of the characterization of $FeMnPO_4$ using the Mapping feature on SEM-EDX. Mapping is often used to determine the distribution of constituent atoms and impurities in a compound sample [9]. In the $FeMnPO_4$ pH 2 precursor, it can be seen that the distribution of the most constituent atoms starts from O, P, and Fe atoms. In the $FeMnPO_4$ pH 2 mapping results, the distribution of Mn atoms is not visible and there are impurity atoms, namely Ti atoms.

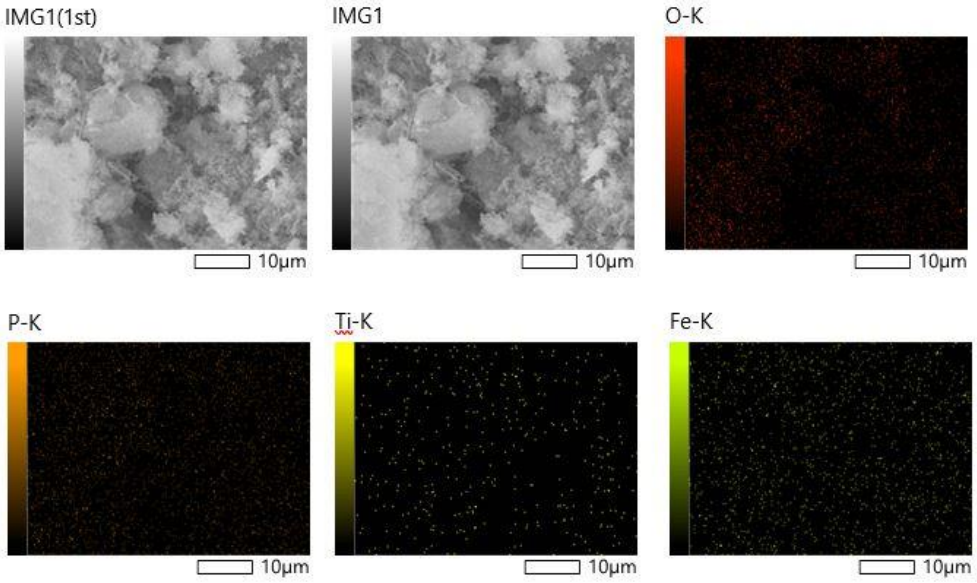

Figure 2. SEM-Mapping of the precursor of $FeMnPO_4$ (pH =2)

Figure 3. SEM test results of $FeMnPO_4$ precursors made with co-precipitation pH 3. Precursor characteristic tests were carried out at 500x, 1000x, and 5000x magnification respectively. Area compared to pH 2 precursor powder. Table 2. EDX test results on $FeMnPO_4$ precursors at pH = 3. In the table, there is a contaminant in the form of elemental Ca with a mass percentage of 3.66 ± 0.98%.

Elements with the largest mass percentage are O elements = 48.44±3.52%, then Fe elements = 25.83±4.40%, then P elements = 15.09±1.65%, and finally Mn elements = 6.97±2.12%, while the percentage of Mn atoms in the pH 3 sample is not yet according to stoichiometric calculations[10].

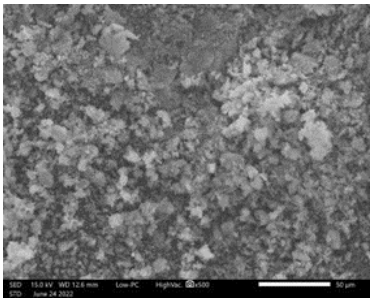

(a)

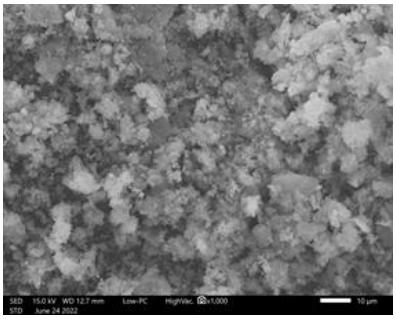

(b)

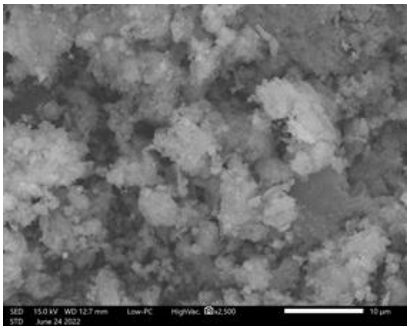

(c)

Figure 3. SEM pattern of the precursor of $FeMnPO_4$ (pH =3) with magnifications (a) 500x, (b) 1000x, and (c) 5000x

Table 2. EDX analysis of $FeMnPO_4$ (pH = 3)

Elements	%Mass	%Atom
O	48,44±3,52	72,16±5,24
P	15,09±1,65	11,61±1,27
Ca	3,66±0.98	2,18±0.58
Mn	6,97±2.12	3,02±0.92
Fe	25,83±4,40	11,02±1,88

Figure 4. the result of characterization of $FeMnPO_4$ pH 3 using the Mapping feature on SEM-EDX. In the $FeMnPO_4$ pH 3 precursor, it can be seen that the distribution of the most constituent atoms starts from O, P, Fe, and Mn atoms. In the results of this $FeMnPO_4$ pH 3 mapping, the impurity is Ti, Ca, and C atoms. The discrepancy in the ratio of the percentage of Mn atoms in the sample is due to the nature of Mn in $MnPO_4$ which easily decomposes into $Mn_3(PO_4)_2$, causing a change in the ratio of Mn and P atoms [11].

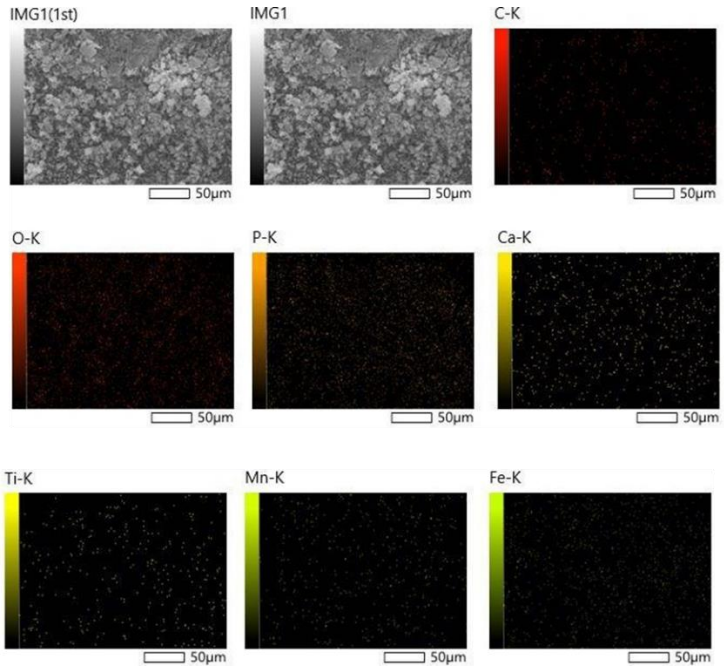

Figure 4. SEM-Mapping of the precursor of $FeMnPO_4$ (pH =3)

Figure 5. SEM test results for $FeMnPO_4$ precursors made with co-precipitation pH 4. Precursor characteristic tests were carried out at 500x, 1000x, and 5000x magnification respectively. When compared according to magnification, it can be seen that precursor powder with pH 4 looks more homogeneous than precursor powder with pH 2 and 3. Table 3, is the result of EDX characterization testing on the $FeMnPO_4$ precursor pH 4 variant. In the table, it is known that the element with the largest weight is element O with mass percentage = 52.96 ± 2.77%, then P = 16.14 ± 1.39 % followed by Mn = 16.01 ± 2.62, and finally, Mn = 0.20 ± 0.60 %. the $FeMnPO_4$ pH 4 sample has a ratio of atomic percentages that resembles stoichiometric calculations [10].

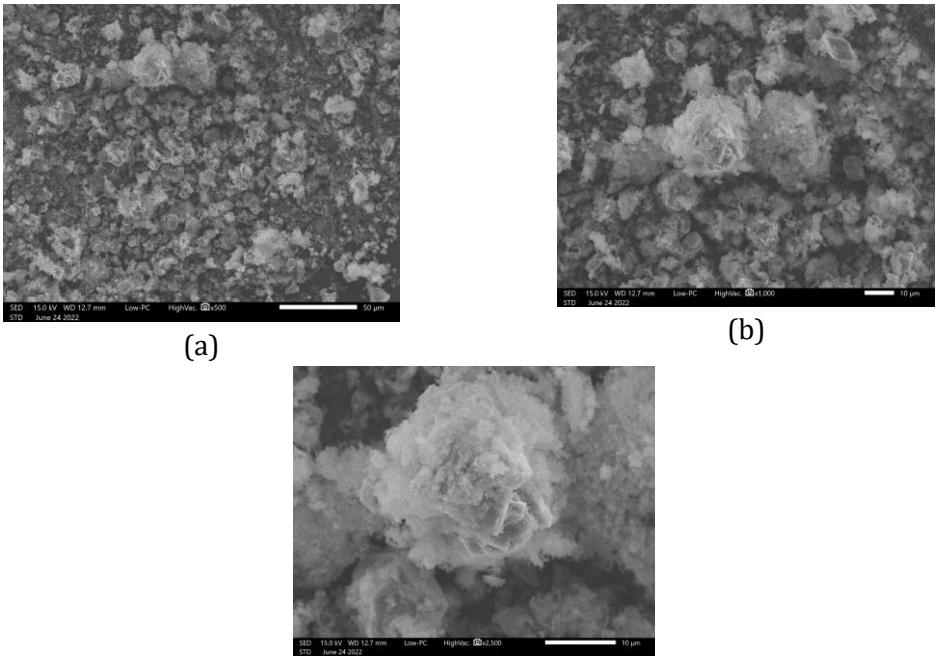

(a) (b) (c)

Figure 5. SEM pattern of the precursor of $FeMnPO_4$ (pH =4) with magnifications (a) 500x, (b) 1000x, and (c) 5000x

Table 3. EDX analysis of $FeMnPO_4$ (pH = 4)

Elements	%Mass	%Atom
O	52.96±2.77	75.42±3.95
P	16.14±1.39	11.87±1.02
Mn	16.01±2.62	6.64±1.09
Fe	14.90±2.76	6.08±1.12

Figure 6. is the result of the characterization of $FeMnPO_4$ pH 4 using the Mapping feature on SEM-EDX. In the $FeMnPO_4$ precursor pH 4, it can be seen that the distribution of the most constituent atoms starts from O, P, Mn, and Fe atoms. In the $FeMnPO_4$ pH 3 mapping results, there are impurity atoms, namely C atoms.

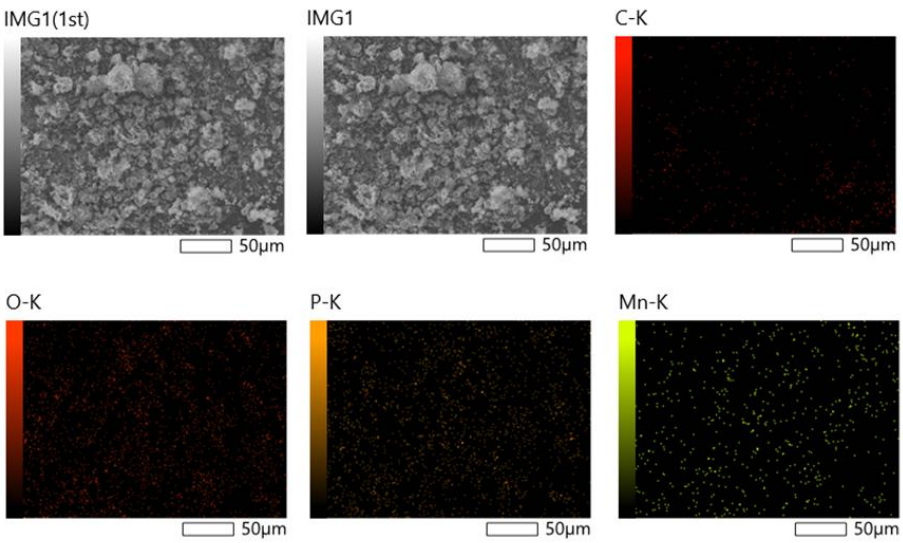

Figure 6. SEM-Mapping of the precursor of $FeMnPO_4$ (pH =4)

The FTIR test is used to determine the bond type of functional groups that interact with infrared. The peaks of 3446 cm-1 and 1637 cm-1 are the bending and stretching bonds of water (H_2O) respectively [12]. The highest absorption peak is seen at the peak of 1047 cm-1 which is a P-O stretching group bond originating from a phosphate ion (PO_4^{-3}). Meanwhile, at the peak of 543 cm-1, there is a stretching Fe-O bond [13].

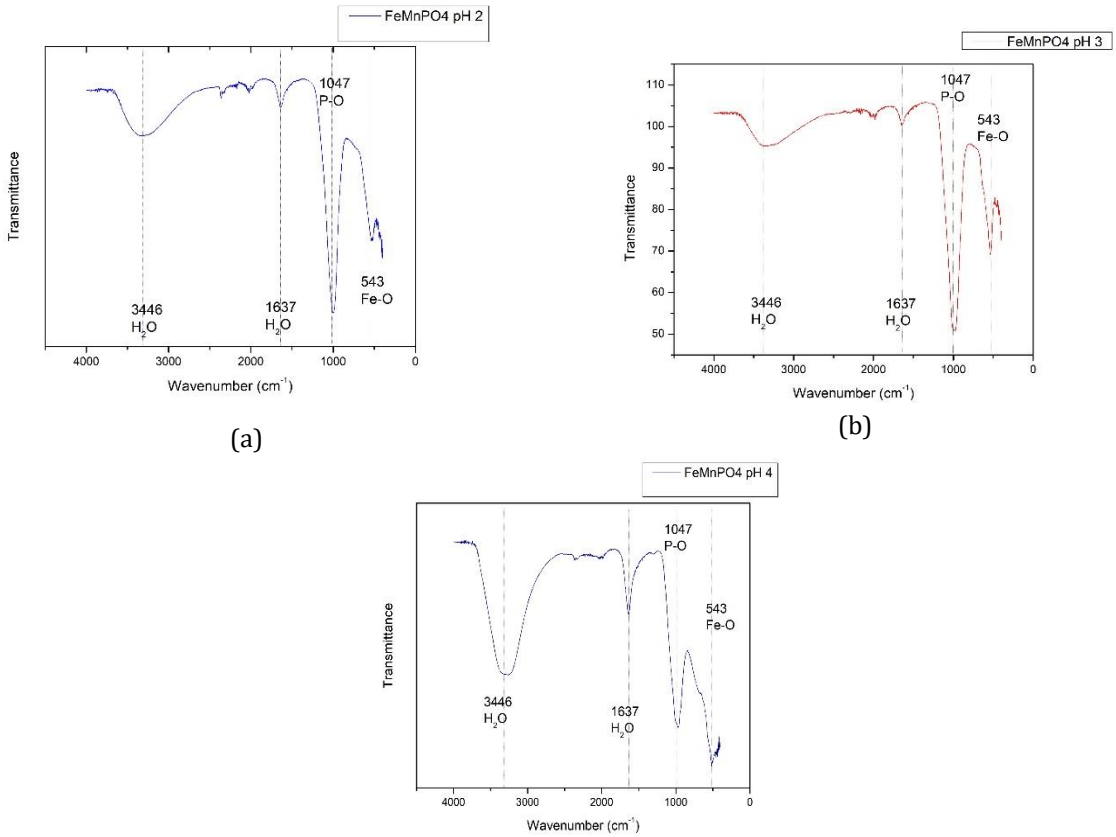

Figure 7. FTIR pattern of the precursor of $FeMnPO_4$ (a) pH = 2 (b) pH = 3 (c) pH =4

The characteristic XRD test is commonly used to determine the phases of crystal formation and crystal defects. On this topic, XRD was carried out at a value of 2θ = 10°-80° with a wavelength of Cu-Kα (1.541874 Å)[14]. The diffractor meter was then matched with the $Fe_{0.5}Mn_{0.5}PO_4$ XRD results carried out by Jongsoon, Kim, et al[15]. In Figure 8, the diffractometer results obtained are an amorphous phase, so the smooth raw data feature is used in the Match! Application. to remove noise and facilitate matching with the $Fe_{0.5}Mn_{0.5}PO_4$ XRD results carried out by Jongsoon, Kim, et al regarding the crystal peaks formed[16].

From matching with the $Fe_{0.5}Mn_{0.5}PO_4$ XRD results carried out by Jongsoon, Kim, et al.[17], it was found that the $FeMnPO_4$ precursor XRD results could not obtain crystalline peaks [18]. Several factors that affect crystal quality are not only crystal defects and particle distribution but are also influenced by the crystallization method and external parameters of the crystallization process such as solvent, anti-solvent, and temperature [19]. Factors that affect the purity of the phase and crystallinity are temperature and long-time stirring.

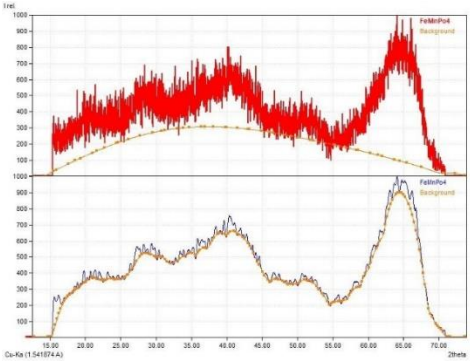

Figure 8. XRD pattern (a) precursor of $FeMnPO_4$ pH 3

Figure 9. DT-TGA test results for each precursor. In this DT-TGA test, each sample was heated to 500°C in an air atmosphere at a temperature rate of 20°C/min. In the TG graph of the pH 2 precursor (Figure 9.a), the initial sample weight was 3.79 grams and then decreased and increased in mass continuously during the temperature of 27.5°C – 339.5°C until the final sample of the precursor pH 2 became 3.03 grams. In the graph of DTA precursor pH 2 (Figure 9.a), the sample undergoes an endothermic reaction at a temperature range of 26°C - 131°C then takes place exothermic in the range of 132-241°C. In the graph of TG precursor pH 3 (Figure 9.b), the initial weight of the sample is 4.4 grams and the final sample weight was 2.69 grams without experiencing peaks of decrease and increase in mass. On the graph of DTA precursor pH 3 (Figure 9.b), the exothermic peak was recorded at temperatures of 70.9°C, and 651.88°C. Meanwhile, the endothermic peak was recorded at 701.95°C. In the pH 4 precursor TG graph (Figure 9.c), the initial sample weight was 15.22 grams and then decreased to 9.95 grams. In the temperature range of 193-200°C, the sample experienced a mass increase of 0.08 grams. In the range of 273-300°C, the sample decreased in mass by 0.42 grams. Loss of mass takes place quickly when in the range of 39.89°C-114.27°C it is 3.82 grams so the sample weight becomes 11.4 grams at 114.27°C. In the graph of DTA precursor pH 4 (Figure 9.c), the sample underwent an exothermic reaction in the range of 40°C-91.73°C and 274.27°C-297.75°C [20].

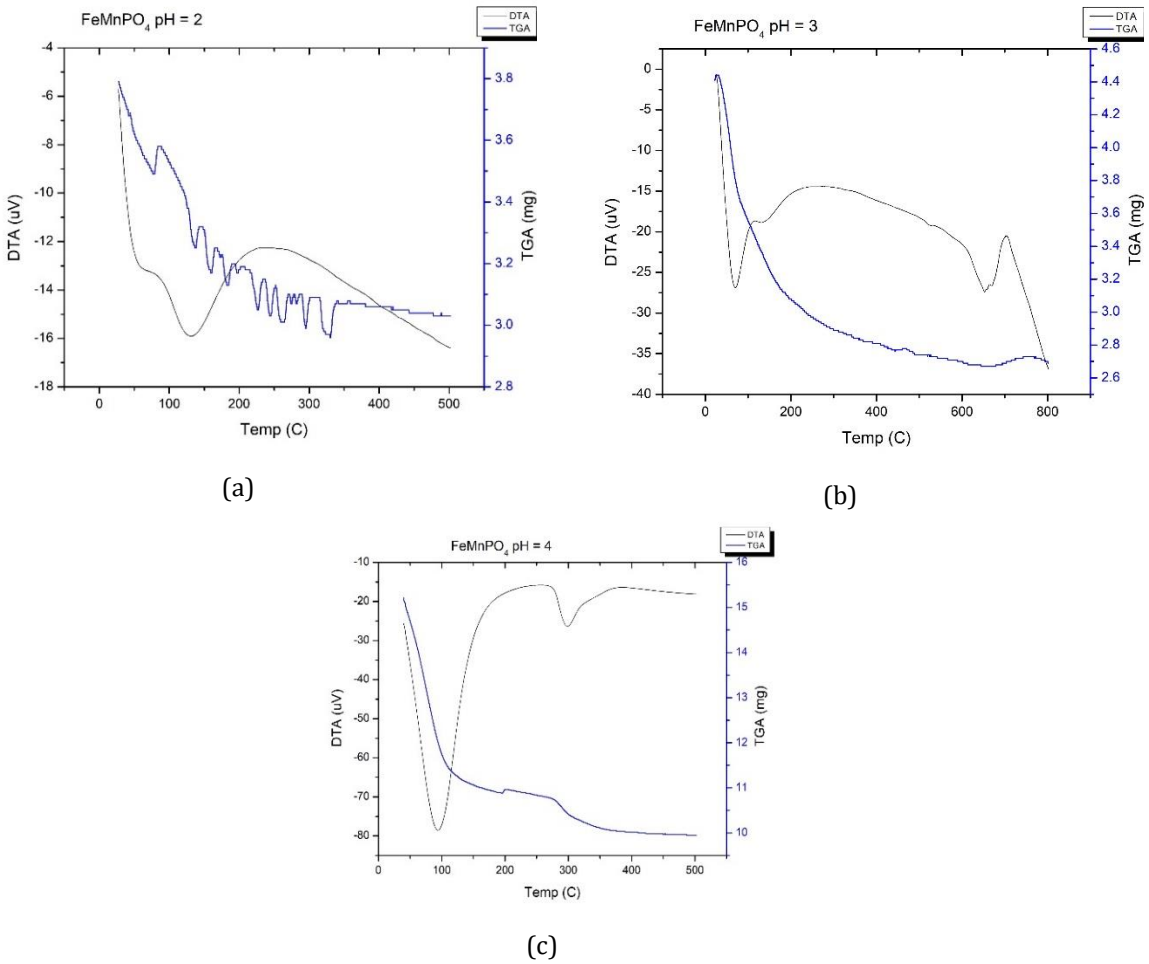

Figure 9. DT-TGA pattern of the precursor of $FeMnPO_4$ (a) pH = 2 (b) pH = 3 (c) pH =4

4. Conclusion

Li-ion batteries (LIB) are todays emerging technology allowing multiple applications from electric vehicles to personal wireless gadgets to be more efficient than before. The development of LIBs towards better performance is necessary. In this study, the preparation of $LiFe_{0.5}Mn_{0.5}PO_4$ precursor was conducted. The synthesis of precursor $Fe_{0.5}Mn_{0.5}PO_4$ (LFMP) was performed by the co-precipitation method. The pH reaction was varied at 2,3, and 4. Based on the results, all pH is able to produce the LFMP precursor. Based on the characterizations, the samples with good particles are obtained at a pH reaction of 4. Based on this evidence, the preparation of LFMP will be cost-effective and will be conducted in future research.

Acknowledgment

The authors are grateful for the research facility provided by the Centre of Excellence for Electrical Energy Storage Technology, Universitas Sebelas Maret.

Author Contributions

Hilmy Naufal Wibowo experimented. Meidiana Arinawati wrote the manuscript with the support Cornelius Satria Yudha and Khairuddin. The final manuscript was edited by Cornelius Satria Yudha. The overall project was supervised by Khairuddin. The final report was committed by all contributors.

References

[1] W. Li *et al.*, "Enhancing high-voltage electrochemical performance," 2020.

[2] C. S. Yudha, A. P. Hutama, M. Rahmawati, and M. Arinawati, "cathode material for high capacity NCA / graphite secondary battery fabrication," pp. 501–510, 2022.

[3] D. Young, J. Kim, J. Moon, and M. Park, "Off-stoichiometric TiO 2- x -decorated graphite anode for high-power lithium-ion batteries," *Journal of Alloys and Compounds*, vol. 843, p. 156042, 2020, doi: 10.1016/j.jallcom.2020.156042.

[4] Q. Cheng, W. M. Chirdon, M. Lin, K. Mishra, and X. Zhou, "Characterization, modeling, and optimization of a single-step process for leaching metallic ions from LiNi 1/3 Co 1/3 Mn 1/3 O 2 cathodes for the recycling of spent lithium-ion batteries," *Hydrometallurgy*, vol. 185, pp. 1–11, 2019, doi: 10.1016/j.hydromet.2019.01.003.

[5] M.-K. Tran, A. DaCosta, A. Mevawalla, S. Panchal, and M. Fowler, "Comparative Study of Equivalent Circuit Models Performance in Four Common Lithium-Ion Batteries: LFP, NMC, LMO, NCA," *Batteries*, vol. 7, no. 3, p. 51, Jul. 2021, doi: 10.3390/batteries7030051.

[6] Z. Liu *et al.*, "Effects of chelating agents on electrochemical properties of Na0.9Ni0.45Mn0.55O2 cathode materials," *Journal of Alloys and Compounds*, vol. 855, p. 157485, 2021, doi: 10.1016/j.jallcom.2020.157485.

[7] J. O. Agunsoye, J. A. Adebisi, S. A. Bello, M. Haris, J. B. Agboola, and S. B. Hassan, "Synthesis of silicon nanoparticles from cassava periderm by reduction method," *Materials Science and Technology 2018, MS and T 2018*, no. January, pp. 701–709, 2019, doi: 10.7449/2018/MST_2018_701_709.

[8] J. Yang, B. Guo, H. He, Y. Li, C. Song, and G. Liu, "LiNi0.5Mn0.5O2hierarchical nanorods as high-capacity cathode materials for Li-ion batteries," *Journal of Alloys and Compounds*, vol. 698, pp. 714–718, 2017, doi: 10.1016/j.jallcom.2016.12.264.

[9] W. Zhuang, J. Ye, Z. Song, G. Yin, and G. Li, "Comparison of semi-active hybrid battery system configurations for electric taxis application," *Applied Energy*, vol. 259, no. November, p. 114171, 2020, doi: 10.1016/j.apenergy.2019.114171.

[10] R. Aisyah, S. T. Samudera, A. Jumari, and A. Nur, "Synthesis of FePO4 Precursor for LiFePO4 Battery Cathode from Used Nickel Plated A3 Steel Battery Shell by Hydrometallurgy Processing," *Energy Storage Technology and Applications*, vol. 1, no. 1, p. 7, 2021, doi: 10.20961/esta.v1i1.56802.

[11] C. Ma, K. Yang, L. Wang, and X. Wang, "Facile synthesis of reduced graphene oxide/Fe3O4 nanocomposite film," *Journal of Applied Biomaterials and Functional Materials*, vol. 15, no. Suppl 1, pp. S1–S6, 2017, doi: 10.5301/jabfm.5000341.

[12] M. Arinawati, A. P. Hutama, C. S. Yudha, M. Rahmawati, and A. Purwanto, "Facile rheological route method for LiFePO4/C cathode material production," *Open Engineering*, vol. 11, no. 1, pp. 669–676, 2021, doi: 10.1515/eng-2021-0068.

[13] H. M. Barkholtz, A. Fresquez, B. R. Chalamala, and S. R. Ferreira, "A Database for Comparative Electrochemical Performance of Commercial 18650-Format Lithium-Ion Cells," *Journal of The Electrochemical Society*, vol. 164, no. 12, pp. A2697–A2706, 2017, doi: 10.1149/2.1701712jes.

[14] B. Sadeghi, R. Sarraf-Mamoory, and H. R. Shahverdi, "Surface modification of LiMn2O4 for lithium batteries by

nanostructured LiFePO4 phosphate," *Journal of Nanomaterials*, vol. 2012, no. May 2015, 2012, doi: 10.1155/2012/743236.

[15] R. Weber, H. Li, W. Chen, C.-Y. Kim, K. Plucknett, and J. R. Dahn, " In Situ XRD Studies During Synthesis of Single-Crystal LiNiO 2 , LiNi 0.975 Mg 0.025 O 2 , and LiNi 0.95 Al 0.05 O 2 Cathode Materials ," *Journal of The Electrochemical Society*, vol. 167, no. 10, p. 100501, 2020, doi: 10.1149/1945-7111/ab94ef.

[16] X. H. Ma *et al.*, "Three-dimensional MnO/reduced graphite oxide composite films as anode materials for high performance lithium-ion batteries," *Ceramics International*, vol. 43, no. 14, pp. 10873–10880, 2017, doi: 10.1016/j.ceramint.2017.05.121.

[17] D. S. Kim, Y. E. Kim, and H. Kim, "Improved fast charging capability of graphite anodes via amorphous Al2O3 coating for high power lithium ion batteries," *Journal of Power Sources*, vol. 422, no. February, pp. 18–24, 2019, doi: 10.1016/j.jpowsour.2019.03.027.

[18] Et. al Sattar, S.R., Ilyas, S., "Recycling of end-of-life LiNixCoyMnzO2 batteries for rare metals recovery," *Environ. Eng. Res.*, vol. 25, pp. 88–95, 2020.

[19] X. Wang, H. Wang, J. Wen, Y. Tan, and Y. Zeng, "Surface modification of LiMn2O4 cathode with LaCoO3 by a molten salt method for lithium ion batteries," *Ceramics International*, vol. 47, no. 5, pp. 6434–6441, 2021, doi: 10.1016/j.ceramint.2020.10.225.

[20] R. Acharya, T. Subbaiah, S. Anand, and R. P. Das, "Preparation, characterization and electrolytic behavior of β-nickel hydroxide," *Journal of Power Sources*, vol. 109, no. 2, pp. 494–499, 2002, doi: 10.1016/S0378-7753(02)00164-7.